The Role of Electrostatics in Protein–Protein Interactions of a Monoclonal Antibody

ARTICLE *in* MOLECULAR PHARMACEUTICS · JUNE 2014

Impact Factor: 4.38 · DOI: 10.1021/mp5002334

molecular pharmaceutics

Article

pubs.acs.org/molecularpharmaceutics

The Role of Electrostatics in Protein−Protein Interactions of a Monoclonal Antibody

D. Roberts,[†] R. Keeling,[†] M. Tracka,[‡] C. F. van der Walle,[‡] S. Uddin,[‡] J. Warwicker,[†] and R. Curtis*[,†]

[†]School of Chemical Engineering and Analytical Science, The University of Manchester, Sackville Street, Manchester M13 9PL, U.K.
[‡]Formulation Sciences, MedImmune Ltd., Aaron Klug Building, Granta Park, Cambridge CB21 6GH, U.K.

Supporting Information

ABSTRACT: Understanding how protein−protein interactions depend on the choice of buffer, salt, ionic strength, and pH is needed to have better control over protein solution behavior. Here, we have characterized the pH and ionic strength dependence of protein−protein interactions in terms of an interaction parameter k_D obtained from dynamic light scattering and the osmotic second virial coefficient B_{22} measured by static light scattering. A simplified protein−protein interaction model based on a Baxter adhesive potential and an electric double layer force is used to separate out the contributions of longer-ranged electrostatic interactions from short-ranged attractive forces. The ionic strength dependence of protein−protein interactions for solutions at pH 6.5 and below can be accurately captured using a Deryaguin−Landau−Verwey−Overbeek (DLVO) potential to describe the double layer forces. In solutions at pH 9, attractive electrostatics occur over the ionic strength range of 5−275 mM. At intermediate pH values (7.25 to 8.5), there is a crossover effect characterized by a nonmonotonic ionic strength dependence of protein−protein interactions, which can be rationalized by the competing effects of long-ranged repulsive double layer forces at low ionic strength and a shorter ranged electrostatic attraction, which dominates above a critical ionic strength. The change of interactions from repulsive to attractive indicates a concomitant change in the angular dependence of protein−protein interaction from isotropic to anisotropic. In the second part of the paper, we show how the Baxter adhesive potential can be used to predict values of k_D from fitting to B_{22} measurements, thus providing a molecular basis for the linear correlation between the two protein−protein interaction parameters.

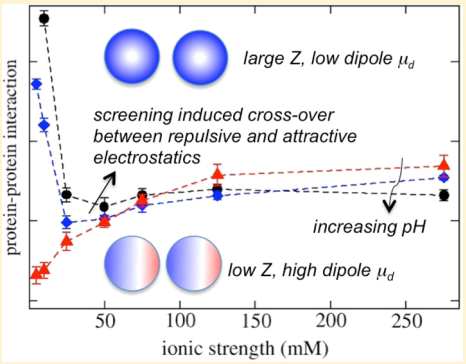

KEYWORDS: *protein−protein interactions, osmotic second virial coefficients, diffusion interaction parameters, monoclonal antibody, electrostatics*

INTRODUCTION

Recent studies of nonspecific protein−protein interactions have been driven by the need for developing stable liquid formulations of antibodies or antibody derived products, which have rapidly become a large market of biotherapeutics. Antibody self-interactions are linked to problems such as protein aggregation,[1−3] liquid−liquid phase separation and opalescence,[4−10] and high viscosities.[11−18] These problems are often exagerated at high protein concentrations, which are often needed in liquid formulations to meet patient dose requirements. Problems can be minimized by manipulating the solution conditions, such as choices of buffers, pH, ionic strength, and the inclusion of other small molecule additives such as sugars, amino acids, and other excipients. A better understanding of protein−protein interactions and how they depend on solution conditions can aid in formulation development by reducing the solvent space to be screened for protein stability.

Weak protein−protein interactions are most commonly characterized in terms of the osmotic second virial coefficient, B_{22}, which provides a direct link to a solvent-mediated interaction between a pair of proteins averaged over their separation and relative orientations. Much of what is known about protein−protein interactions was learned from studies motivated by the discovery of a link between B_{22} and crystallizability; in order for protein crystallization to be possible, the value of B_{22} must fall in a window of interaction strength. More recently, studies have shown that in low ionic strength solutions, the value of B_{22} is correlated with the protein aggregation behavior.[2,3,19−22] Even for solutions where proteins are more likely to form partially folded aggregation prone states, lowered aggregation propensities occur when the protein has a high net charge. In this case, repulsive double-layer forces increase the colloidal stability of the protein. Conversely, in solutions near to the isoelectric pH (pI) of the protein, attractive electrostatic interactions between proteins have been linked to increased aggregation propensities.[12] Other studies have correlated increased viscosities of concentrated protein solutions with attractive protein−protein interactions

Received: March 28, 2014
Revised: May 15, 2014
Accepted: June 3, 2014

dx.doi.org/10.1021/mp5002334 | *Mol. Pharmaceutics* XXXX, XXX, XXX−XXX

characterized in dilute protein solutions under the same solvent conditions.[12−18]

These studies highlight the utility of protein−protein interaction measurements in dilute solutions, but an improved understanding of protein solution behavior is needed for predicting concentrated solution properties from dilute meausurements of protein−protein interactions.[23,24] As a starting point, there is a need for being able to separate out the different energetic contributions to the molecular interactions. In the context of protein formulations, studies have suggested the presence of an adhesive protein−protein interaction when it is masked due to the presence of long-range double layer forces.[12,25,26] In solutions at low ionic strength, the net protein−protein interaction measured in dilute solution is repulsive, however, a short-ranged attraction has still been inferred indirectly from rheological characterization in more concentrated protein solutions, where the average separation of proteins is significantly reduced such that the short-ranged attraction is entropically favored. In addition, electrostatic repulsion can prevent aggregation at low protein concentration, but not at high concentrations where the short-ranged attraction becomes significant.[27]

Because most measurements such as B_{22} only provide an averaged protein−protein interaction, deconvoluting the interaction into individual contributions requires matching the measurements to interaction models. Often the molecular-level interpretation gained from the studies depends on the level of coarse-graining and the force field used to describe the protein and the solvent. Detailed calculations using all-atomistic descriptions of proteins and an implicit water model indicate that protein−protein interactions are more likely anisotropic in a manner similar to specific protein−protein interations because the interaction is dominated by a small number of highly attractive configurations determined by shape complementarity and van der Waals forces.[28−30] In this case, the energetically favored orientations are on the order of tens of k_BT.[30] The latter view is consistent with the intuition that interactions should be anisotropic in order to trap the protein in an orientationally constrained configuration needed for crystallization. For globular proteins, the crystal structure is representative of the solution protein conformation, in which case protein surfaces buried in crystal contacts should reflect the protein−protein interactions formed in solution. However, simulations using an explicit model for water indicate that the calculated strength of orientationally restricted interactions corresponding to lysozyme−lysozyme crystal contacts is only a couple k_BT.[31] Interactions of this magnitude are not large enough to constrain protein orientational interactions in solution. The latter is supported by the finding that a mutation to hemoglobin significantly alters the protein crystal solubility, although the liquid−liquid phase separation remains unaffected indicating that anisotropic interactions formed in the crystal are not the same as those sampled in solution.[32] A mutation study of an antibody suggested that protein−protein interactions depended on the properties of a charged patch, suggesting that electrostatic interactions, rather than shape complementarity, control the protein−protein sampling in solution at low ionic strength.[33] These large discrepancies in estimating the interaction energetics reflect the difficulty in deconvoluting the protein−protein interaction into individual contributions.

The aim of this work is to carry out a detailed protein−protein interaction study as a function of pH and ionic strength to provide more insight into the molecular origin of protein−protein interactions for monoclonal antibodies. The measurements are matched to a simplified interaction model, based on a Baxter adhesive potential and a double layer force taken from Deryaguin−Landau−Verwey−Overbeek (DLVO) theory. We also carry out ζ-potential measurements and calculations of the protein electrostatic properties to provide more insight into the origin of protein−protein interactions. The model is not meant to provide an exact description of the protein−protein interaction but instead is a tool that allows us to separate out the effects of electrostatics from excluded volume forces and other short-ranged interactions. Deviations from the model provide insights into whether interactions are anisotropic and the key stumbling blocks to building a more realistic, predictive model for protein−protein interactions.

Recent investigations of protein−protein interactions have characterized them in terms of an interaction parameter k_D, which is given by the slope of the mutual diffusion coefficient versus protein concentration. Experimentally, studies have shown a linear relationship between k_D and B_{22} indicating that the parameter can be used as a surrogate for B_{22}.[2,17,34] The advantage is that k_D can be measured using a multiwell plate dynamic light scattering plate reader, which leads to much more rapid measurements and minimal sample consumption compared with approaches for assessing the osmotic second virial coefficient using static light scattering. Here, we quantify protein−protein interactions from k_D measurements and then benchmark them against B_{22} meaurements for selected solution conditions. The observed correlation between B_{22} and k_D is not surprising in that k_D is related to protein−protein interactions through well-established relationships.[35−38] Using the latter approaches combined with the simplified protein model, we show how both interaction parameters provide equivalent information and thus provide a molecular basis for the correlation.

EXPERIMENTAL SECTION

Sample Preparation. mAb1 is an IgG1 with sequence molecular weight equal to 144.8 kDa. The mAb1 was obtained as a pure liquid formulation at a concentration of 41 g/L in an aqueous solutions containing 25 mM histidine buffer and 7% w/v sucrose at pH 6.0. The extinction coefficient of mAb1 is 1.42 mL/(g cm).

A size exclusion high performance liquid chromatography run with an online Heleos multiangle light scattering detector (from Wyatt Technology) was used to check for the presence of aggregates in the formulation. An injection of 25 μL of the mAb1 at 10 g/L was used. The step was carried out using a TSKgel HPLC column (G3000SWXL, 7.8 mm ID × 30 cm, 5 μm particle size) at a flow rate of 1 mL/min with a mobile phase composed of 100 mM sodium phosphate buffer containing 100 mM disodium sulfate at pH 6.8.

Before each experiment, 4 L of the buffer solution was prepared using a buffer concentration that fixed the ionic strength at either 5, 10, or 25 mM as calculated according to the Henderson−Hasselbach equation. All buffer solutions were filtered through a vacuum filtration unit using a 0.2 μm PES membrane (Stericup, Thermo Scientific Ltd., UK). The mAb1 formulation was concentrated to approximately 150 g/L using an Amicon Ultracentrifuge filter of 30K MWCO (Merck-Millipore Ltd., Ireland) and then placed in a Slide-A-Lyser dialysis cassette with a maximum volume of 3 mL and a 10K MWCO (Thermo Scientific Ltd., U.K.). The dialysis cassette was placed in 2 L of a dialysis buffer and stirred for 4 h. The

dx.doi.org/10.1021/mp5002334 | Mol. Pharmaceutics XXXX, XXX, XXX−XXX

dialysis buffer was then exchanged, and the dialysis was continued overnight. The dialyzed sample and the dialyzate were then saved and used for all subsequent sample dilutions.

Static Light Scattering. Static light scattering is used here for determining the osmotic second virial coefficient, B_{22}. For a system containing protein, water, and salt, the light scattering equation is given by[39−41]

$$\frac{Kc(\partial n/\partial c)^2_{T,\mu_w,\mu_s}}{R_\theta} = \frac{1}{Mk_BT}\left(\frac{\partial \Pi}{\partial \rho}\right)_{T,\mu_w,\mu_s} \quad (1)$$

where Π is the osmotic pressure of the protein solution over that of the salt solution, subscripts w and s correspond to water and salt, respectively, R_θ is the measured excess Rayleigh scattering ratio of the protein solution over the solvent, M is protein molecular weight, ρ is the protein number concentration, which is related to protein masss concentration c by $\rho = N_A c/M$ with Avogadro's number represented by N_A. K is the light scattering constant given by $2\pi^2 n_0^2/(N_A\lambda^4)$, where n_0 is the refractive index of the solvent, and λ is the wavelength of the light. $(\partial n/\partial c)_{T,\mu_w\mu_s}$ is the refractive index increment of the protein solution measured at constant chemical potential of the water and salt, μ_s and μ_w. In solutions at low salt concentration

$$\left(\frac{\partial n}{\partial c}\right)_{T,\mu_w,\mu_s} \approx \left(\frac{\partial n}{\partial c}\right)_{T,p,m_s} \quad (2)$$

The refractive index increment at constant pressure p and salt molality m_s has been measured extensively for protein solutions and is equal to approximately 0.185 L/g.

The osmotic compressibility can be calculated from the derivative of the virial expansion

$$\frac{1}{k_BT}\left(\frac{\partial \Pi}{\partial \rho}\right)_{T,\mu_w,\mu_s} = 1 + 2b_{22}\rho + O(\rho^2) \quad (3)$$

where b_{22} is the osmotic second virial coefficient, which provides the link to the molecular level protein−protein interactions. The terms omitted from the sum on the right side of the equation are related to higher order virial coefficients. Thus, the second virial coefficient is strictly defined as the slope of osmotic compressibility plot at zero protein concentration. In practice, the virial coefficient should only be calculated from the linear part of the plot at low protein concentrations. Substituting the result into eq 1

$$\frac{Kc}{R_\theta} = \frac{1}{M} + 2\frac{b_{22}N_A}{M^2}c \quad (4)$$

Often, measured values of b_{22} are reported in units of mL·mol/g^2, which corresponds to the definition

$$B_{22} = \frac{b_{22}N_A}{M^2} \quad (5)$$

In a light scattering experiment, R_θ is measured for a series of samples with varying protein concentrations. A plot of the left side of eq 4 versus c yields a slope equal to $2B_{22}$ and the inverse of the y-intercept equal to M.

A Wyatt miniDAWN TREOS 3 angle detector was used for the static light scattering experiments. The instrument uses a 60 mW GaAs diode laser with vertically polarized light at a wavelength of 658 nm. There is no angle dependent scattering when the particle size is less than 1/20th the wavelength of light. In these instances, the best data quality is obtained using the 90° detector to minimize the effect of dust particulates. Measurements were made using a flow cell. Samples were delivered using the Calypso, an automated syringe pump manufactured by Wyatt Technology. The Calypso contains three programmable syringe pumps used to generate very precise step gradients in concentrations. The flow from each syringe pump goes through an in-line 0.1 μm pore size membrane. A static mixer is used to mix the streams after the filtration step before the sample enters the flowcell. In a typical light scattering experiment, the protein solution dissolved in only the dialysis buffer at a bulk concentration of 16 g/L is placed in syringe pump 1. The dialysis buffer is placed in syringe pump 2, and syringe pump 3 contains a salt solution prepared in the same dialysis buffer. The Calypso was then programmed to generate a series of experiments. Each virial coefficient determination was based on two experiments, (1) using step gradients of increasing protein concentration and (2) with gradients of decreasing protein concentration. In each experiment, protein concentration is varied in equal step changes between concentrations of 2 and 8 g/L at fixed salt concentration. Protein concentrations were determined from dilution factors calculated from the relative flow rates of the pumps. The concentrations were verified from absorbance readings at 280 nm measured with a Waters 2487 absorbance detector connected in series to the outlet of the light scattering flowcell. We used a variable path length flowcell in order to accurately determine the protein concentration. The path length of the flowcell was set to 0.05 cm such that the absorbance of the protein solutions falls within the range over which the Beer−Lambert law is valid.

Dynamic Light Scattering. In a dynamic light scattering experiment, macromolecular diffusion coefficients are quantified from fitting to the measured intensity autocorrelation function over time. The function $C(t)$ is given by $C(t) = Ag(t)^2 + B$, where A is an instrument-dependent optical constant and B is a background term, determined for each sample in the limit of large delay times.[42] For a monodisperse solution where the wavelength of light is much larger than the size of the scattering particle, the first order autocorrelation function $g(t)$ is related to

$$g(t) = e^{-Dq^2t} \quad (6)$$

where q is the magnitude of the scattering vector ($\mathbf{q} = 4\pi n_0 \sin(\theta/2)/\lambda$); θ is the scattering angle). The main quantity measured in dynamic light scattering experiment is the translational diffusion coefficient of the particle D, which controls the decay time for correlations in the fluctations of scattered light. For monodisperse solutions, D can be determined from fitting $g(t)$ to the measured autocorrelation function. However, protein solutions always contain a small amount of impurities, either irreversibly formed aggregates, a small fraction of other protein impurities, or dust particles. Accounting for these requires fitting the correlation function to a population distribution. For polydispersed solutions, $g(t)$ is given by

$$g(t) = \frac{\sum_i \rho_i M_i^2\, e^{-D_i q^2 t}}{\sum_i \rho_i M_i^2} \quad (7)$$

which corresponds to a z-weighted average over all sizes of particles at molecular wight M_i and number density ρ_i. Relating the measured correlation function to the diffusion coefficient is

dx.doi.org/10.1021/mp5002334 | Mol. Pharmaceutics XXXX, XXX, XXX−XXX

an ill-conditioned problem because different distributions can yield the same measured $g(t)$. A general approach to overcoming this problem for samples with mononodal distributions is to use the cumulant expansion. In this case, the natural logarithm of the correlation function is fit to a second order polynomial in the delay time

$$\ln g(t) = -q^2 D_z t + \frac{q^4 t^2}{2}(\delta D)_z^2 \tag{8}$$

where the subscript z denotes the z-average of the property. The first order coefficient in the expansion corresponds to the z-average of the diffusion coefficient. The second moment of the distribution is equal to the second order coefficient, which is the z-average in the fluctuations of the diffusion coefficient; larger flucuations are related to broader size distributions. A measure of the polydispersity in the sample is often defined as $P = (\delta D)_z^2/D_z^2$, which is equal to zero for monodisperse samples.

The measured diffusion coefficient can be expanded in a series about protein concentration

$$D = D_0[1 + k_D c] \tag{9}$$

D_0 corresponds to the infinite dilution value of the diffusion coefficient, which is often reported in terms of the hydrodynamic radius, R_h, using the Stokes–Einstein relationship

$$R_h = \frac{k_B T}{6\pi\eta D_0} \tag{10}$$

Here R_h is the radius of a sphere that has the same diffusion coefficient as the protein and η is the solvent viscosity. The parameter k_D reflects the interactions between proteins, which controls their collective motion. Experimental studies have already shown a monotonic correlation between k_D and B_{22} indicating that the parameter provides a direct measure of protein–protein interactions. A discussion on the theoretical connection between k_D and the protein–protein pair potential of mean force, W, is given later in the text when we introduce the protein–protein interaction model.

Diffusion coefficients were measured using a DynaPro PlateReader (Wyatt, Santa Barbara, CA) at a laser wavelength of 838.88 nm with 30 μL samples in a 384 well plate. Each measurement included ten 5 s acquistions. For each solvent condition, six samples were measured with equally spaced protein concentrations and a maximum protein concentration of ~25 g/L. For each protein concentration, measurements were carried out in triplicate and then averaged. Cumulants analysis was done using the Wyatt Technology Dynamics Software. Values of polydispersity, P, greater than 0.1 indicate relatively broad size distributions and are not considered when analyzing the data. All measurements were performed at 25 °C.

Zeta (ζ) Potential Measurements. ζ-Potential was measured by massively-parallel phase analysis light scattering (MP-PALS) using a Mobius mobility instrument manufactured by Wyatt Technology. The velocity of charged particles under an applied electric field leads to a frequency (or Doppler) shift in the scattered light, which is used to determine the electrophoretic mobility by MP-PALS. The instrument contains a dynamic light scattering detector, which allows for simultaneous determination of electrophoretic mobility and particle diffusion coefficient. A 70 mW solid state laser at a wavelength of 532 nm provides light source and 30 detector channels are used to improve the sensitivity and speed of the measurement. Assuming the protein behaves as a uniformly charged spherical particle, the Henry equation can be used to relate the electrophoretic mobility μ_e to the ζ potential

$$\zeta = \frac{3\eta}{2\epsilon_0 \epsilon f(\kappa a)}\mu_e \tag{11}$$

where a is the particle radius, ϵ_0 is the vacuum permittivity, ϵ is the dielectric constant of the medium, and κ is the inverse Debye–Huckel screening length, λ_{DH}

$$\kappa = 1/\lambda_{DH} = \sqrt{2e^2 N_A I/(\beta\epsilon\epsilon_0)} \tag{12}$$

I is the ionic strength of the electrolyte solution, inverse temperature is given by $\beta = 1/(k_B T)$, and e is the electronic charge. $f(\kappa a)$ is the Henry's function. The Henry's function can be approximated by

$$f(\kappa a) = 1 + \frac{1}{2}\left[1 + \left(\frac{2.5}{\kappa a[1 + 2\exp(-\kappa a)]}\right)\right]^{-3} \tag{13}$$

Henry's equation is valid for values of $\zeta < 50$ mV, which correponds to when the polarization of the diffuse double layer is small and the surface conductivity is negligible.[43]

THEORY

Electrostatic Calculations. The electrostatic charge and potential distribution were calculated for a homology model of mAb1 using an in-house program.[44] We report percentage of solid angle covered by the positive and negative surface potentials corresponding to magnitudes of the potential greater than 25 mV or less than −25 mV, respectively. In addition, contours of the surface potential at 25 mV and −25 mV were used to determine the sizes of the largest positively charged and negatively charged patches. The patch size corresponds to the percentage of solid angle coverage. A comparative model was made based on PDB id 1hzh, with subsequent adjustment to make the two Fab-Fc orientations approximately symmetric.

Protein–Protein Interaction Model. The main motivation for carrying out the complementary B_{22} studies is that the parameter provides a direct link to protein–protein interactions, whereas the link to k_D measurements is less well established especially for particles with nonspherical shapes. Thus, we initially focus on intrepreting the B_{22} studies in terms of a simplified protein–protein interaction model and then examine the transferability to describing the k_D measurements. The exact relation between the osmotic second virial coefficient and the protein–protein interactions, as characterized in terms of the protein pair potential of mean force, is given by

$$b_{22} = \frac{1}{16\pi^2}\int_\Omega \int_0^\infty [1 - g(r, \Omega)] r^2 \, dr \, d\Omega \tag{14}$$

where r is the center-to-center separation between a pair of proteins and $g(r,\Omega)$ is the pair distribution function given by

$$g(r, \Omega) = \exp[-\beta W(r, \Omega)] \tag{15}$$

The protein pair potential of mean force $W(r,\Omega)$ is an interaction free energy averaged over all the solvent and cosolvent degrees of freedom. Equation 14 contains a multiple integral over the set of angles defining the relative orientations between a pair of proteins Ω.

For rigid molecules, the potential of mean force can be further broken up into the sum of an excluded volume contribution, $W^{ex}(r,\Omega)$, and the sum of all other longer-ranged interactions denoted by $W^{soft}(r,\Omega)$. The excluded volume term

dx.doi.org/10.1021/mp5002334 | Mol. Pharmaceutics XXXX, XXX, XXX–XXX

is equal to infinity for the set of separations and relative orientations in which the pair of proteins overlap with each other and zero otherwise. The integral over the excluded volume term in eq 14 yields

$$b_{22} = b_{22}^{ex} + \frac{1}{16\pi^2}\int_{\Omega'}\int_{d_c(\Omega')}^{\infty}[1 - \exp(-\beta W^{soft}(r, \Omega))]r^2 \, dr \, d\Omega_c \quad (16)$$

where Ω_c denotes the set of orientations in which the proteins do not overlap with each other, and d_c is the center-to-center separation between proteins at contact. b_{22}^{ex} is the excluded volume contribution to the osmotic second virial coefficient, which corresponds to the volume that is made inaccessible to the center of a protein due to the presence of the interacting partner averaged over all their relative orientations. The difference $b_{22}^{soft} = b_{22} - b_{22}^{ex}$ often referred to as the *energetic* part of the protein−protein interaction accounts for all interactions except the entropic excluded-volume contribution.[45] If the difference is less than zero the net energetic interaction W^{soft} is attractive, whereas a difference greater than zero reflects a net repulsive interaction. A recent study carried out the detailed integration given by eq 14 to determine what level of coarse graining was needed in order to capture the excluded volume calculated from all-atomistic description of the protein based on its crystal structure.[46] The key finding is that the contribution can be approximated by the excluded volume of a sphere with a radius given by the experimentally measured hydrodynamic radius of the protein, in which case

$$b_{22}^{ex} = \frac{16}{3}\pi {R_h}^3 \quad (17)$$

The approximation holds true for a range of proteins with degrees of complexity ranging from single domain proteins through to a monoclonal antibody.

The energetic contributions to protein−protein interactions can be further broken down according to the range of the force. The longer-ranged interaction arises from electrical double layer forces, whereas short-ranged forces can be composed of all types including dispersion forces, solvation forces such as hydrophobic or hydration, or other forms of electrostatic interactions such as salt bridges. The molecular origin of short-ranged interactions between proteins are not well-known as highlighted in the Introduction of this article. Here, we do not attempt to relate the short-ranged protein−protein interactions to a physical model but instead use an adjustable parameter to reflect the adhesive forces between proteins or configurations where the separation between surfaces of proteins are close enough (within a solvent layer) to be considered in contact. We use the Baxter adhesive potential w^{sr}, which is the limiting case of a square well potential when the well depth goes to infinity as the width goes to zero, chosen in such a way that the contribution of the interaction to B_{22} remains constant. As such, the advantage of using this model is that only one parameter is needed to describe the interaction. The potential given by

$$w^{sr}(r) = -\epsilon \quad \text{for} \quad \sigma < r < \sigma(1 + \Delta) \quad (18)$$

where σ corresponds to an effective hard sphere diameter, is taken in the limit of $\Delta \to 0$ where ϵ is defined by

$$\epsilon = \frac{1}{\beta}\ln\left(1 + \frac{1}{12\tau}\right) \quad (19)$$

where τ corresponds to the strength of the adhesive force between the particles. In the Baxter limit, the second virial coefficient becomes

$$B_{22}^{sr} = -\frac{B_{22}^{ex}}{4\tau} \quad (20)$$

Previous studies have shown the Baxter model can capture the generic phase behavior and osmotic compressibility for globular proteins solutions in moderately concentrated salt solutions.[47,48] In addition, small-angle X-ray scattering studies have indicated that the protein−protein interaction has a short-range on the order of one-tenth the diameter of the protein,[49] and the static structure factor curve can be accurately fit using the Baxter potential.[50]

The energetic part of the protein−protein interaction is given by the sum of a short ranged term and a long-ranged electrical double layer force. In this case,

$$B_{22}^{soft} = B_{22}^{sr} + B_{22}^{el} \quad (21)$$

As a starting point to describe the double layer force between proteins, we use DLVO theory. In this approach, the protein is treated as a uniformly charged sphere immersed in a solvent, where the ions are treated as point charges and the water is a continuum characterized by the relative dielectric permittivity of water equal to 78.4. The protein−protein electrostatic repulsion occurs due to an osmotic repulsive force when the electrical double layers overlap, because the local concentration of ions in the double layer is greater than the ion concentration in the bulk. As such, the range of the force is related to the thickness of the double layer, which is characterized by the inverse screening length, κ^{-1}. Analytical solutions to the double layer force between two charged spheres only exist in certain limits. Of relevance to this study is an approximate form derived using the Debye−Huckel approximation and in the limit of $\kappa a < 5$[51]

$$\beta w^{el}(r) = \frac{Z^2\lambda_B}{(1 + \kappa a)^2}\frac{\exp[-\kappa(r - 2a)]}{r} \quad (22)$$

Here, Z corresponds to the protein valency or the effective charge on the protein per electronic charge, e, and includes the ions bound in the Stern layer surrounding the protein; a is equal to the distance from the protein center to the outer Helmholtz plane (OHP), which separates the diffuse layer from the Stern layer. The Bjerrum length, $\lambda_B = e^2/(4\pi\beta\epsilon\epsilon_0)$ is the ion−ion separation when the Coulomb energy is equal to thermal energy, k_BT, equal to ∼0.7 nm for water at room temperature. The model potential has provided accurate fits to the pH and ionic strength trends of B_{22} for protein solutions at low ionic strength (below 200 mM).[52−54]

Deviations to DLVO theory are greatest at pH values near to the pI, where the electrostatic repulsion is weakened due to lowering the net charge. The anisotropic distribution of charge becomes significant and is often linked to the presence of attractive electrostatic interactions, which have been observed for chymotrypsinogen[28] and for antibodies in slightly basic solutions close to their pI.[13,21,25,33] Nevertheless, DLVO theory provides a good starting point to interpret the interactions in solutions at pH removed from the pI. Here, we show that deviations from DLVO theory provide strong evidence for the presence of anisotropic electrostatic interactions.

Relating Protein−Protein Interactions to k_D. There is a less direct correspondence between the potential of mean force

dx.doi.org/10.1021/mp5002334 | Mol. Pharmaceutics XXXX, XXX, XXX−XXX

and the interaction parameter k_D. All measurements were performed in the long-time scale regime, where the characteristic time scale probed by the DLS experiment is much greater than the velocity correlation time for the protein. In this limit, fluctuations in local particle concentration can be described by the diffusion equation

$$\frac{\partial \rho}{\partial t} = D\nabla^2 \rho(r, t) \tag{23}$$

Particle diffusion is controlled by a chemical potential gradient, the drag force exerted on a particle from the solvent, and interparticle hydrodynamic forces as mediated by the solvent. Calculating hydrodynamic forces requires solving the Navier–Stokes equations for incompressible flow about the particles. Various appoximations have been used to solve these equations and then solve for k_D by matching the solution to eq 23. Here we use the result obtained by Felderhof,[35] in which case, the value of k_D is given by

$$k_D = k_V + k_O + k_A + k_S + k_{FD} \tag{24}$$

where the virial term k_V is the thermodynamic contribution driving diffusion. k_V is related to the osmotic second virial coefficient by $k_V = 2B_{22}M$

$$k_V = -6B_{22}^{ex}M \int_0^\infty [g(x) - 1]x^2 \, dx \tag{25}$$

The effects of hydrodynamic interactions are also related to the potential of mean force according to

$$k_O = 3B_{22}^{ex}M \int_0^\infty [g(x) - 1]x \, dx \tag{26}$$

which is the Oseen term,

$$k_A = 6B_{22}^{ex}M \int_0^\infty \left[\frac{9}{8}\frac{1}{(2x)^6} - \frac{5}{4}\frac{1}{(2x)^4}\right] g(x)x^2 \, dx \tag{27}$$

and

$$k_S = \frac{75}{8}B_{22}^{ex}M \int_0^\infty \frac{g(x)}{(2x)^5} \, dx \tag{28}$$

are short-range hydrodynamic interactions, and

$$k_{FD} = 1 \tag{29}$$

is the force dipole part. In the above integrals, the substitution of $x = r/(2a)$ has been made to make the representations simplistic. There have been several studies that have fit the interaction parameters to DLVO type potentials for lysozyme solutions and found realistic values for the net charge and Hamaker constant.[36,55] In other studies, the contribution of the soft part of the interaction has only been included in the Oseen and virial terms, which follows on from a study demonstrating that the short-range hydrodynamic interactions arising from the Yukawa potential are negligible.[56] With the latter approach applied to solutions of a monoclonal antibody, DLVO parameters fit to the value of k_D agreed closely to the fits obtained from the correponding B_{22} values measured by static light scattering.[52]

When we include the short-range Baxter adhesive potential in the model to account for short-range forces, the interaction parameter is given by the sum

$$k_D = k_D^{ex} + k_D^{el} + k_D^{sr} \tag{30}$$

The excluded volume terms is given by the sum over all virial and hydrodynamic terms to give[35,56]

$$k_D^{ex} = 0.39B_{22}^{ex}M \tag{31}$$

The double layer term only contains the Oseen and virial contributions

$$k_D^{el} = k_O^{el} + k_V^{el} \tag{32}$$

which are evaluated using a lower limit of integration given by the effective hard sphere diameter, $2a$. The short-range term is

$$k_D^{sr} = k_O^{sr} + k_V^{sr} + k_A^{sr} + k_S^{sr} \tag{33}$$

The model described above only accounts for repulsive double layer forces, and no term is included for a long-ranged electrostatic attraction.

RESULTS AND DISCUSSION

Electrostatic Properties. We first report the results of the ζ-potential measurements, which are used to probe the charged properties of the protein. The ζ-potential corresponds to the electrical potential at the slip plane between the protein and the solvent.[43] The effective charge of the protein can be related to the ζ potential using Debye–Huckel theory assuming that the OHP and the slip plane are located at the same position

$$Z_\zeta = \frac{4\pi\epsilon_0\epsilon(1 + \kappa a)\phi_d}{e} \tag{34}$$

where ϕ_d is the electrical potential evaluated at the beginning of the diffuse layer (or at the OHP). Within this model Z_ζ is the fixed charge arising from the ionized groups on the protein and the ions bound in the Stern layer.

We measured the ζ-potential for 1 g/L mAb1 solutions at an ionic strength of 25 mM containing sodium actetate buffer at pH 5 and 6.5 and containing tris-chloride buffer and sodium chloride at pH 8 and 9. In addition, measurements were carried out as a function of pH for a solution containing 1 g/L mAb1 and 10 mM NaCl. In the latter measurement, the samples were obtained by titrating a solution of mAb1 at an initial pH of 4.5 with dilute NaOH dissolved in 10 mM NaCl. All the measured potentials were less than 20 mV and correspond to conditions where Henry's equation (eq 11) is valid. The results are reported in terms of Z_ζ shown in Figure 1 as a function of pH. The error bars correspond to the standard error taken over measurements of three independent runs. The values reported here for Z_ζ at pH 6.5 are in the same range as those reported in other ζ-potential studies of antibodies at pH 6 in histidine-hydrochloride buffer at ionic strength between 15 and 20 mM.[15,34] There is an expected decrease in Z_ζ due to reducing the net positive charge arising from the protein ionizable groups. In acidic solutions, the values of Z_ζ are lower in magnitude than the theoretical calculations of the protein charge shown in the inset to Figure 1, which is consistent with the findings of other studies.[15,34,57,58] The fixed charge on the protein surface can be either calculated from theoretically derived pK_a values or measured using a potentiometric titration. In either case, the value does not account for the charges arising from ions bound in the Stern layer, which contribute to the measured ζ-potential. Thus, the lower value of Z_ζ relative to charge estimated from the titration curve indicates preferential binding of chloride ion to the positively charged protein groups. This result is consistent with other ζ-potential studies; for instance, in sodium chloride solutions of BSA, the excess

dx.doi.org/10.1021/mp5002334 | Mol. Pharmaceutics XXXX, XXX, XXX–XXX

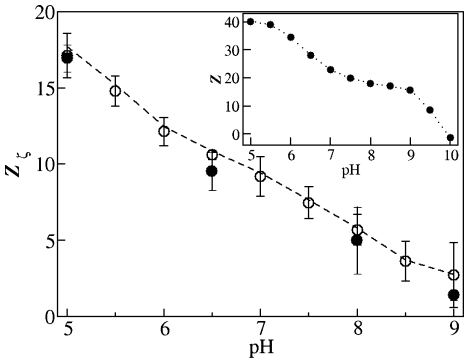

Figure 1. Plot of charge estimated from ζ-potential measurements. Open circles correspond to solutions of mAb1 containing approximately 10 mM NaCl with no buffer, where the protein charge Z_ζ has been calculated using the Debye–Huckel approximation, and the dashed line corresponds to the full solution of the Poisson–Boltzmann equation. Closed symbols correspond to solutions containing sodium acetate buffer at an ionic strength contribution of 25 mM at pH 5 and at pH 6.5. Solutions at pH 8 and 9 are at an ionic strength of 25 mM containing sodium chloride and a tris chloride buffer at an ionic strength contribution of 10 mM and 5 mM, respectively. The inset contains the theoretical calculation of charge Z arising from protein ioinizable groups.

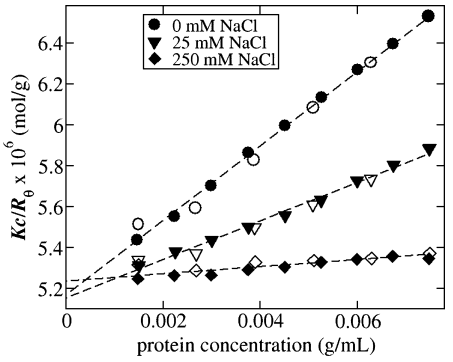

Figure 2. Experimental static light scattering data obtained in solutions at pH 5.75 containing sodium acetate buffer at an ionic strength of 25 mM for solutions with varying NaCl concentration. Closed symbols and open symbols correspond to data obtained with decreasing and increasing gradients of protein concentration, respectively.

number of bound chloride ions over bound sodium ranged from 20 at pH 4 to 10 ions at pH 5.3, the isoelectric point of BSA.[58] Because similar trends in ion specific binding are observed across many different proteins,[59−62] a similar amount of preferential anion binding is expected to occur with the mAb1 investigated here. The measured values of Z_ζ at fixed pH are similar for the solutions at 25 and 10 mM ionic strength. Thus, there are no discernible effects on the protein net charge when sodium is replaced by tris in alkaline solutions or when chloride is replaced by acetate in acidic solutions.

For a monovalent salt solution, Debye–Huckel theory corresponds to the limit $\beta e\zeta_d < 1$, in which case the Poisson–Boltzmann equation can be linearized when solving for the mobile ion distribution about the protein. For the solutions at pH 5, the measured value of $\beta e\zeta_d \approx 1$. As a consequence, we have checked the validity of eq 34 by using a semiempirical equation that provides an accurate approximation of the nonlinear Poisson–Boltzmann equation when calculating the ion distribution about a charged sphere[51]

$$Z_\zeta = (\kappa a)\frac{a}{\lambda_B}\left[2\sinh\left(\frac{e\beta\phi_d}{2}\right) + \frac{4}{\kappa a}\tanh\left(\frac{e\beta\phi_d}{4}\right)\right] \quad (35)$$

The calculations of Z_ζ using eq 35 are shown by the dashed line in Figure 1. The largest deviations occur at pH 5, but the relative difference is only 3% indicating that the Debye–Huckel theory provides a reasonable estimate within the experimental error of the measurement.

pH and Ionic Strength Dependence of Protein–Protein Interactions for mAb1. Next we characterized the ionic strength and pH dependence of the osmotic second virial coefficient, which is related to the protein pair potential of mean force by eq 14. Positive values of the parameter reflect repulsive protein–protein interactions, whereas negative values correspond to attractive forces. In Figure 2 are shown experimental data obtained for an experiment using a buffer of sodium acetate with an ionic strength contribution of 25 mM at pH 5.75. A B_{22} measurement is obtained at fixed salt concentration by collecting the light scattering data from a series of samples with a decreasing gradient in protein concentration (given by the closed symbols in Figure 2), followed by a series of samples with increasing concentration (open symbols in Figure 2). A linear regression of the combined data set was used to calculate the slope from the plot (see eq 4) equal to $2B_{22}$; reported error bars correspond to the standard error in the slope estimation. The molecular weight of mAb1 is equal to the inverse of the regressed intercept. The measured values of the molecular weight from all experiments fell in the range of 190 to 200 kDa, which is greater than the sequence molecular weight estimated to be 148 kDa. A measured monomer molecular weight equal to 145 kDaA was obtained for the monomer fraction from an SEC-MALLS step indicating the refractive index increment of 0.185 mL/g is accurate. Only a small fraction of trimer (less than 0.1% w/v) eluted before the monomer peak during the SEC-MALLS step. The larger weight-average molecular weight observed in the batch light scattering experiment is thus due to a small population of irreversibly formed aggregates, which are filtered out by the guard column and SEC step. The aggregates were not resolved in the dynamic light scattering experiment indicating that the aggregate hydrodynamic size cannot be greater than approximately five times the monomer value. This is consistent with the finding that aggregates are removed by the guard column of a SEC step, but not by filtering through a syringe top filter with a 0.02 μm pore size. The effect of irreversibly formed aggregates on the measured B_{22} value is expected to be negligible since the aggregates occur at a small relative mass fraction.[54]

The value of k_D is obtained from the slope of a plot of the normalized mutual diffusion coefficient D/D_0 versus protein concentration. Sample data are shown in Figure 3 for experiments using a 25 mM sodium acetate buffer at pH 5.75 with different NaCl concentrations. The infinite dilution coefficient D_0 was first obtained from the intercept of the best fit line to a plot of D versus protein concentration. The hydrodynamic radius R_h was calculated from the Stokes–Einstein relation using a viscosity equal to 0.89 cP, which corresponds to water at 25 °C. The measured values of R_h from all the experiments were in the range between 5.0 and 5.3 nm, which is similar to other DLS studies of IgG1 antibodies.[2,18] The error bars reported on the values of k_D correspond to the standard error in the slope estimate from plotting D/D_0 versus

dx.doi.org/10.1021/mp5002334 | Mol. Pharmaceutics XXXX, XXX, XXX–XXX

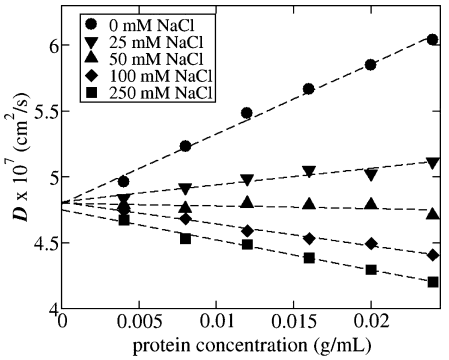

Figure 3. Plots of mutual diffusion coefficient as a function of protein concentration obtained at pH 5.75 with sodium acetate buffer at an ionic strength contribution of 25 mM for solutions with varying NaCl concentration.

protein concentration. In some instances, error bars are not visible when they have the same size or are smaller than the corresponding symbols used in the plots. Polydispersities less than 0.05 were obtained for most DLS measurements indicating a very small amount of large molecular weight impurities. A regularization analysis indicated that the data is fit by a single mononodal distribution, which is consistent with the low measured polydispersity.

In Figure 4 is shown measured values of B_{22} for mAb1 under mildly acidic conditions as a function of ionic strength. In each

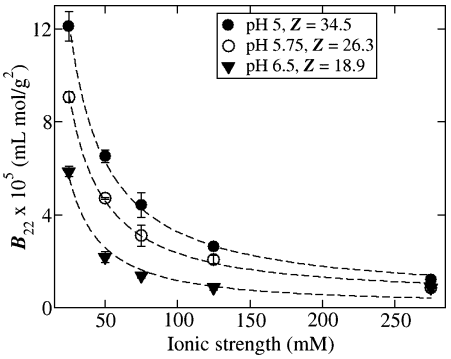

Figure 4. Plot containing experimental data for B_{22} and lines of best fit as a function of ionic strength for solutions containing sodium chloride at pH 5, 5.75, and 6.5 with sodium acetate buffer at an ionic strength contribution of 25 mM. The values of Z corresponding to the best fit are shown in the legend.

case, the ionic strength contribution of the sodium acetate buffer is 25 mM. Protein−protein repulsion is reduced with increasing ionic strength at fixed pH or by increasing pH at fixed ionic strength. The curves shown in the figure are the fits to the protein−protein interaction model, which includes contributions from the excluded volume, a short ranged adhesive force, and a double-layer repulsion. For each pH value, the model contains only two fit parameters, the protein net charge given by Z, which is shown in the figure legend, and the sum $B_{22}^{ex} + B_{22}^{sr}$. The purpose of using the model is to discriminate between electrostatic interactions and short-ranged forces. The fitting is sensitive to the data over the ionic strength range of 25−100 mM where there is a sharp decrease in B_{22} values due to screening of the electrostatic interactions. The physical meaning of the fit parameters are discussed later in the text. The good agreement obtained for the fitting indicates that the double layer potential provides an adequate model for capturing the ionic strength dependence of B_{22}. Treating the antibody as a uniformly charged sphere seems to be an oversimplification of the protein shape and surface properties. The reason such an approach can be used has been discussed previously when describing the ionic strength dependence of lysozyme−lysozyme interactions.[53] B_{22} values much greater than the excluded volume contribution indicate that the protein−protein interactions are long-ranged and repulsive. Under these conditions, there will be no bias to the relative orientations sampled by a pair of proteins, so that the averaging process will correspond to the averaged protein surface properties, rather than the distribution of surface charge. This approach is supported by a finding that proteins undergo rapid rotational motion,[63] and other studies, where DLVO theory has been applied to obtain accurate fits in protein solutions at low ionic strength and at pH values removed from the isoelectric point.[36,52−55]

The strength of the short-ranged attraction is reflected by the values for the fit parameters, B_{22}^{sr}. At pH 5 and 5.75, the value of B_{22}^{sr} is equal to -6.1×10^{-5} mL·mol/g^2 for pH 5 and 5.75, whereas at pH 6.5, the value is equal to -6.5×10^{-5} mL·mol/g^2. In obtaining these values, we have used the calculated value of B_{22}^{ex} equal to 6.7×10^{-5} mL·mol/g^2 for an R_h equal to 5.2 nm (see eq 17). These estimates of the short-ranged interactions are calculated with a model including the electric double layer potential. However, at an ionic strength of 275 mM, we expect that the electrostatic interactions are weak and a similar range to the adhesion force as the screening length is on the order of a solvent layer. This is also supported by the small change in B_{22} values when ionic strength increases from 125 to 275 mM. Because the forces act over a similar range, it is not possible to separate the contributions to the potential of mean force. Furthermore, the DLVO potential is not expected to be a realistic representation of the electrostatic interactions at moderate ionic strength, where the soft part of the protein−protein interaction is attractive and likely anisotropic.[28,29] A more realistic quantification of the short ranged forces is given by the experimentally measured value of B_{22} minus the excluded volume term. With either approach, however, we find that there is a significant short-ranged attraction at moderate ionic strength. When electrostatic interactions are not included, the short-ranged interaction is independent of changing pH from 5 to 6.5, whereas, a small pH dependence is observed when electrostatics is included in the model.

In Figure 5 is shown the measured and fit k_D values obtained in solutions of mAb1 with sodium acetate buffer at pH 5, 5.75, and 6.5 and for solutions at pH 7.25 using a tris chloride buffer with a contribution to the ionic strength equal to 10 mM. Similar trends to those found in the B_{22} studies are observed, where at fixed pH, the effect of increasing ionic strength is to screen the protein−protein repulsion, and the effect of increasing pH is to lower the double layer repulsion from reducing the protein net positive charge. As with the B_{22} studies, for each pH value, two parameters, Z and the sum of the contributions from the short-ranged adhesion and excluded volume terms, $k_D^{sr} + k_D^{ex}$, are determined by fitting the ionic strength dependence of k_D to eq 30. The fit curves agree well with the experimental values for solutions at pH 6.5 and below. In solutions at pH 7.25, the k_D values at moderate ionic strength are overestimated by the fitting, perhaps providing evidence for the presence of attractive protein−protein interactions, which are not captured by DLVO theory. In

dx.doi.org/10.1021/mp5002334 | Mol. Pharmaceutics XXXX, XXX, XXX−XXX

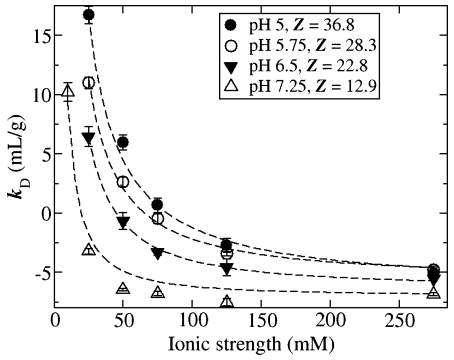

Figure 5. Plot containing experimental data for k_D and lines of best fit as a function of ionic strength for solutions containing sodium chloride at pH 5, 5.75, and 6.5 with sodium acetate buffer at an ionic strength of 25 mM and at pH 7.25 with a tris chloride buffer at an ionic strength of 10 mM.

Table 1 below are shown the different estimations of protein charge. The differences between the values obtained by fitting

Table 1. Tabulated Values of Protein Charge

pH	Z_ζ	Z^a	Z^b
5.0	17.1	34.5	36.8
5.75	13.4	26.3	28.3
6.5	10.6	18.9	22.8

[a]Values of Z fit to the B_{22} data. [b]Values of Z fit to the k_D data.

to the k_D or to the B_{22} measurements are small, indicating that eqs 25−28 provide an accurate representation of k_D in terms of protein−protein interactions. Previous studies have shown the equivalence of using either B_{22} or k_D measurements to regress protein−protein potential of mean force parameters for lysozyme.[36,53,55] However, the error associated with assuming the protein is spherical is expected to be much smaller for a globular protein such as lysozyme, compared with that for a multidomain antibody. The findings presented here along with a similar study provide evidence that such an approach works equally well for antibodies.[52]

Small angle X-ray scattering studies of proteins indicate that the form of the double layer potential does not match the measured structure factor and very often leads to unrealistic values of the fit parameters.[64] However, DLVO potentials are able to accurately capture the ionic strength dependence of k_D or B_{22}, indicating that the model still provides a semiempirical approach to account for the contribution of the averaged electrostatic interaction to the net protein−protein potential of mean force. It is thus still of value to rationalize the protein charge estimated from the DLVO potential in terms of the measured ζ-potential. In the Supporting Information, we have determined the effect of approximations used in DLVO theory on the value of Z needed to match the measured values of B_{22} in solutions at pH 5. The fit value of Z must fall in a window corresponding to the values obtained when solving the double-layer potential using a constant potential and constant charge boundary conditions. The minimum value is equal to 26.7, which is much greater than the value determined from the ζ-potential measurements equal to 17.1. Within the approximations that the protein is a uniformly charged sphere, we would expect that the values agreed with each other since the ζ-potential corresponds to the electrical potential at the beginning of the diffuse layer, ϕ_D, which is also the determining potential in the DLVO model. However, assuming a spherical shape and a uniform charge distribution for the antibody will introduce error in the estimation of Z_ζ. The uncertainty becomes apparent when we compare the same electrophoretic property determined by different methods. For instance, for a series of mAbs, the measured isoelectric points by capillary electrophoresis were consistently less by 0.5 to 1.0 pH units than those determined from electrophoretic light scattering.[34] For this pH difference, the change in protein charge can be on the order of 10; thus drawing definitive conclusions based on the absolute magnitude of Z_ζ is not possible. Nevertheless, the finding that the fit value of Z is much greater than Z_ζ appears to indicate that the double layer potential underpredicts the protein−protein repulsion; if the value of Z_ζ is used in the DLVO potential, the value of B_{22} will be much less than the measurement. This underestimation cannot be reconciled by including charge anisotropy in the potential model, because this will always lead to a lower estimate in the protein−protein repulsion since the attractive configurations in the B_{22} calculation have a greater weighting. Other possibile sources of error include neglecting contributions from Donnan equilibria or neglecting higher order contributions in the virial expansion, both of which will lead to a larger value of B_{22}.[65]

Within DLVO theory, the main effect of changing ionic strength is to screen repulsive double layer forces. However, there are many instances, where protein−protein interactions become more repulsive (or less attractive) with inceasing ionic strength from 10 to 100 mM.[21,33,66−70] Over this range, the main effect of salt is to alter electrostatic interactions, in which case, the observed pattern of protein−protein interactions reflects the presence of attractive electrostatic forces. This behavior was first studied in detail for chymotrypinsogen at pH values between 5.2 and the protein isoelectric pH of about 8.[69] The presence of attractive electrostatic interactions indicate configurational biasing of attractive orientations between proteins, although the forces that control the sampling are difficult to identify. The chymotrypsinogen data formed the basis for detailed computational studies in which the integral for B_{22} was approximated using all-atomistic representations of the protein based on crystal structure data.[28] The main finding was that the protein−protein interactions are dominated by a few highly attractive orientations correponding to a high degree of surface complementarity, where electrostatics only contribute to the energy of the interactions. In this case, attractive electrostatics results from the charge asymmetry in the interacting configurations. More recently, attractive electrostatics observed in antibody systems have been rationalized by considering the distribution of charge on an antibody implying that electrostatics control the configurations that are being sampled by interacting proteins.[13,21,25,33] For instance, mutagenesis was used to disrupt a negatively charged patch in the V_L chain of a mAb. The change altered the protein−protein interaction from attractive to repulsive at an ionic strength of 15 mM demonstrating that attractive electrostatics originate from having oppositely charged patches on the same protein.[33]

In order to examine the effect of mAb1 charge anisotropy, we have measured B_{22} and k_D values at alkaline pH values. The results are shown in Figures 6 and 7. A tris chloride buffer has been used at an ionic strength contribution of 10 mM at pH 8 and an ionic strength of 5 mM for solutions at pH 8.5 and 9. For these plots, the lines are only drawn as guides for the eye since it is not possible to fit the data to a DLVO potential. At

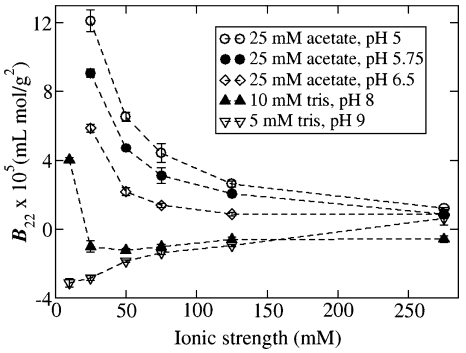

Figure 6. B_{22} values measured as a function of ionic strength for solutions containing sodium chlroide at pH 5, 5.75, and 6.5 with sodium acetate buffer at an ionic strength of 25 mM and at pH 8 and 9 with tris chloride buffer at an ionic strength of 10 and 5 mM, respectively.

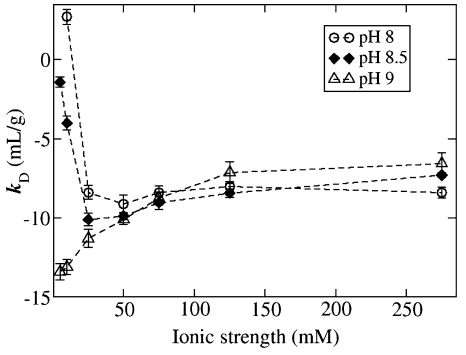

Figure 7. k_D values obtained as a function of ionic strength for solutions with tris chloride at an ionic strength of 5 mM for pH 8.5 and 9 and at an ionic strength of 10 mM for pH 7.25 and 8. NaCl was used to adjust the total ionic strength of all solutions.

pH 9, there is a substantial increase in the values of B_{22} or k_D with increasing ionic strength. The trend reflects what is expected for the screening of attractive electrostatic interactions. Because B_{22} values are less than the excluded volume contribution, adding salt is reducing protein−protein attraction rather than enhancing protein−protein repulsion. Also, we find a novel nonmonotonic dependence of the protein−protein interaction with increasing ionic strength from 10 to 275 mM at pH values of 8 and 8.5. This behavior occurs at a pH intermediate of where repulsive and attractive electrostatics have been observed. Thus, for solutions at pH 8 and 8.5, it is likely that the initial increase of ionic strength screens repulsive double layer interactions, leading to attractive electrostatics, which are then screened by further increased ionic strength. For the solutions at pH 7.25, there is also a very shallow minimum in k_D values at an ionic strength of 125 mM. While difficult to detect from the experimental data, it is more clear when comparing the fit of the potential of mean force model to the experimental data. The fit curve overestimates the experimental k_D values (see Figure 5) indicating the presence of an additional ionic strength dependent electrostatic attraction. Within our knowledge, this maximum in protein−protein attraction occurring at relatively low ionic strength (less than 200 mM) has only been observed directly from B_{22} studies of β-lactoglobulin,[70] which correlated well with the large dipole moment of β-lactglobulin at pH 4 indicating that the nonmonotonic dependence arises from the charge anisotropy.

The observed nonmonotonic dependence of protein−protein interactions implies that repulsive double layer forces are greatest at low salt concentration, whereas attractive electrostatics dominate at an intermediate ionic strength. This explanation follows directly from considering electrostatic screening functions, where the screening of a monopole−monopole interaction is greater than that of a monopole−dipole interaction, which in turn is greater than that of a dipole−dipole interaction.[71,72] A numerical study to determine the potential of mean force between charged-dipolar spheres indicated that the nonmonotonic dependence occurred over a small window of charge for a sphere with dipole moment equal to 380 D.[71] With decreasing charge from 5 to 3, the maximum becomes more pronounced and shifts toward lower ionic strength. Further lowering charge makes the maximum more shallow until it disappears at a charge equal to 1. The same qualitative behavior is observed here, where at pH 7.25 there is a shallow maximum at an ionic strength of 125 mM, which shifts to 50 mM at pH 8 and becomes more pronounced at pH 8.5, where the maximum occurs at 25 mM. The nonmonotonic behavior disappears in solutions at pH 9, conditions where mAb1 still carries a net positive charge as is evident from the ζ-potential measurements. The significant difference with respect to the charged-dipole model is that the peak in attraction occurs at a higher ionic strength for the protein solutions. A shift to higher ionic strengths is expected if a short-ranged nonelectrostatic attraction is included in the charged-dipole model. Thus, it is likely that the minimum in the electrostatic attraction is controlled both by electrostatics and by the presence of a short-ranged protein−protein attraction, which will make the nonmonotonic behavior much more pronounced. This cooperativity has been observed in a simulation study examining the electrostatic steering between lysozyme and several neutral protein fragments, in which case, the presence of van der Waals forces significantly enhanced the free energy of protein heteroassociation.[73]

The nonmonotonic behavior of protein−protein interactions has been observed indirectly in the context of protein cloud point temperatures, which correspond to the temperature onset of a liquid−liquid phase separation. The trends in temperature cloud points at fixed protein concentration reflect changes to protein−protein interactions, in which case, an increase in a cloud point temperature reflects an increase in protein−protein attraction. Studies of lysozyme have found a maximum in the cloud point temperature with increasing ionic strength for some salts.[74,75] The protein−protein interaction pattern inferred from these studies differs qualitatively from our observations in that the maximum occurs at a higher ionic strength and there is a continuous decrease in the cloud point temperature above the maximum. Both these phenomena provide strong indications that the behavior is not due to screening electrostatic interactions. However, a more recent cloud point temperature study of a mAb has found a similar trend to what we observed here.[5] In that study, with increasing pH from 5.3 to 6.6 for potassium chloride solutions, the maximum in the cloud point temperature shifted from an ionic strength of 120 to 50 mM and became more pronounced reflecting a much stronger protein−protein attraction. In addition, the maximum disappeared in solutions at pH 7.1 indicating the presence of only attractive electrostatic interactions. While this type of behavior has not been observed for other protein solutions, a similar phenomena has been observed in the context of protein−polyelectrolyte interactions.[76] A maximum in protein−polyion

dx.doi.org/10.1021/mp5002334 | Mol. Pharmaceutics XXXX, XXX, XXX−XXX

binding affinity is observed in the range of ionic strengths between 5 and 30 mM. The maximum in binding occurs at a pH where the protein and the polyion have the same net charge. As such, the behavior has been rationalized by the competition between repulsive electrostatics at low ionic strength and attractive interactions between the polyion and an oppositely charged patch on the protein surface. Because this type of behavior has been oberved for a range of protein−polyion pairs, we similarly expect that the nonmonotonic behavior in protein−protein interactions should occur for other proteins, especially in solutions near to the protein isoelectic point.

In order to quantify the anisotropic charge distribution, in Figure 8 we have plotted the percentage of the surface

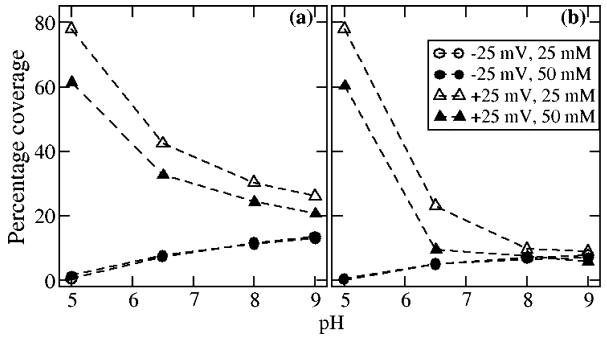

Figure 8. Plots of the percentage coverage of (a) total surface with positive potential and negative potential and (b) largest positively charged patch and largest negatively charged patch. Cut-offs of 25 mV and −25 mV are used for definining positively and negatively charged potentials.

containing positive potential greater than 25 mV and that containing a negative potential less than −25 mV. These potentials are chosen because the electrostatic energy of a point charge at this potential is approximately $1k_BT$. The contours of the potential cut-offs have been used to define the largest positive and largest negative patch for each pH value. The most dramatic effect on mAb1 electrostatic properties is oberved between pH 5 and pH 6.5 as the fraction of the positively charged surface decreases by a factor of 2 and a negative patch appears at pH 6.5. When the pH is further increased from 6.5 to 8, the size of the negatively charged patch remains relatively constant whereas the largest positive patch coverage decreases from 20% to 10% of the protein surface. Definitive conclusions about the origin of attractive electrostatics cannot be drawn from considering the how the patch sizes change with pH.

More details can be gained from visualizing the electrical potentials as shown in Figure 9. At pH 5, the entire surface is covered by the positive potential, which extends much further into the solvent than any of the other pH values. When the pH is increased to 6.5, a patch of negative charge becomes apparent in the hinge region of the protein, and the location of the positive patch contour is much closer to the protein surface. The presence of the negative patch might be linked to the electrostatic attraction observed in the experimental studies. However, the largest change in the electrotatic potential map occurs when pH is changed from 5 to 6.5, whereas much smaller differences occur between pH 6.5 and 8. The latter corresponds to the pH range over which the measured electrostatic interactions change from repulsive to attractive. The most notable change in the potential map is a reduction in

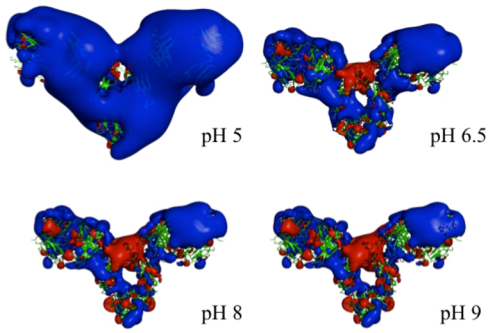

Figure 9. Plots of positive and negative potential as a function of pH. The surface is contoured for absolute values of the potential equal to 25 mV.

the positive patch to a size similar to the negative patch at pH 8. This observation might indicate that at pH 6.5, an interaction between the oppositely charged patch is energetically unfavorable because the outside perimeter of the positive patch is repelled by the positive potential surrounding the negative patch. At pH 8, this unfavorable interaction could be mitigated since the positive region neighboring the negative patch and the size of the positive patch are both significantly reduced, so that there would be no repulsive barrier to forming the attractive interactions. These observations are purely subjective at this point; understanding the origin of the electrostatic interactions will require detailed energetic sampling of the relative orientations between proteins, which will be made more complicated by the interdomain flexibility of the antibody.

Relationship between k_D and B_{22}. In order to explain the correlation between k_D and B_{22}, we first need to express k_D in terms of the adhesive parameter τ, by carrrying out the integrals in eqs 25−28 using the definition of the Baxter potential to give

$$k_V^{sr} = -0.50\tau^{-1}B_{22}^{ex}M \quad (36)$$

$$k_O^{sr} = 0.25\tau^{-1}B_{22}^{ex}M \quad (37)$$

$$k_A^{sr} = -0.03\tau^{-1}B_{22}^{ex}M \quad (38)$$

and

$$k_S^{sr} = 0.023\tau^{-1}B_{22}^{ex}M \quad (39)$$

The equations are written in terms of B_{22}^{ex} to provide a quick estimate of the contribution of the term relative to the effect of excluded volume, $k_D^{ex} = 0.39B_{22}^{ex}M = 3.8$ mL/g for mAb1. Thus, in the absence of any protein−protein attraction, the value of k_D will always be positive. The largest contributions to k_D^{sr} are from a negative virial term, which is double the magnitude of a positive Oseen term. As a consequence, the adhesion force provides a negative net contribution to k_D. The correlation between B_{22} and k_D can be expressed as

$$k_D = 0.39B_{22}^{ex}M - 0.256\tau^{-1}B_{22}^{ex}M \quad (40)$$

or

$$k_D = 0.39B_{22}^{ex}M - 1.024[B_{22}^{ex} - B_{22}]M \quad (41)$$

The contribution of excluded volume relative to the short-range adhesion attractive term is smaller for k_D than for B_{22}; as a consequence, at moderate ionic strength, the values of k_D are negative while those of B_{22} remain positive. Thus, if the

dx.doi.org/10.1021/mp5002334 | Mol. Pharmaceutics XXXX, XXX, XXX−XXX

protein−protein interaction is composed of only short-ranged attractive interactions, according to eq 41, the correlation plot between k_D and B_{22} has a slope close to 1.

The Oseen and virial terms also provide a much larger contribution to k_D^{el} than any other terms. An analytical relation can be gained from considering the limit of weak interactions, in which case[56]

$$k_O^{el} = -\frac{k_V^{el}}{2 + 1/(\kappa a)} \tag{42}$$

In the limit of large κa, the relation $k_O^{el} = -0.5k_V^{el}$ is the same as that obtained for adhesive interactions (see eqs 36 and 37). This result is not surprising because large κ corresponds to when electrostatic interactions are short-ranged due to ionic screening. Thus, the correlation between B_{22} and k_D is independent of the form for the potential of mean force as long as the interaction is short-ranged.

For solutions at high ionic strength, it does not make sense to delineate between electrostatic and short-ranged forces; instead, the electrostatic interactions should also be contained in the adhesive parameter. This limit corresponds to the data taken at 275 mM ionic strength ($\kappa a = 3.1$), which are shown in Figure 10. The closed circles correspond to the experimentally

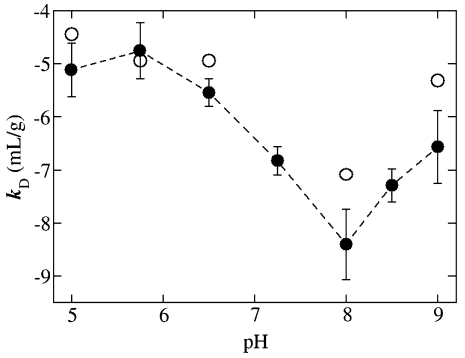

Figure 10. Black circles correspond to experimental k_D values obtained for solutions at 275 mM ionic strength and open circles are predictions based on B_{22} measurements and an interaction model given by the sum of an excluded volume force and the adhesive potential.

measured k_D values, whereas the open circles are the predictions from the model. The adhesion parameter is determined from fitting to the experimental B_{22} data without including electrostatic interactions in the potential of mean force model. The fit value of τ is then used to estimate the value of k_D as represented by the open symbols in Figure 10. The close agreement between measurement and calculation indicate that the model is capturing the generic behavior of a short-ranged attraction between proteins. The approximation that the antibody shape is a sphere with radius equal to the hydrodynamic value is accurate when calculating the value of B_{22}^{ex}. However, this approximation works well because the averaging process used in calculating B_{22} is similar to averaging the rotational degrees of freedom during the translational motion, which is characterized by the infinite dilution value of the diffusion coefficient.[46] Because the Oseen interaction parameter is calculated by an integral weighted by r instead of r^2 as occurs for the virial term, it does not necessarily follow that the excluded volume contribution to the Oseen term can be approximated as a sphere with size R_h. More detailed calculations, which are beyond the scope of this work, would be required to determine the effect of shape anisotropy on the contributions to each interaction parameter.

In Figure 11 is shown the experimental and predicted correlation of k_D with $B_{22}M$. The solid line corresponds to an

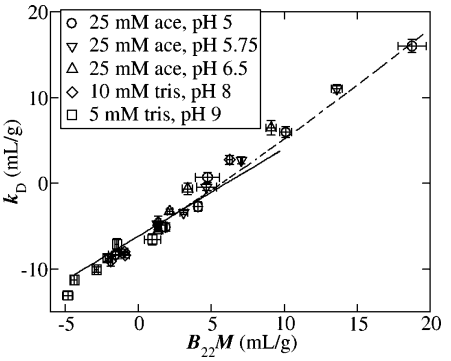

Figure 11. Plot containing correlation of k_D with B_{22} for solutions containing sodium chlroide at pH 5, 5.75, and 6.5 with sodium acetate buffer at an ionic strength of 25 mM and at pH 8 and 9 with tris chloride buffer at an ionic strength of 10 and 5 mM, respectively. Solid line corresponds to predicted correlation when the interaction contains only an excluded volume and an adhesion force. The dashed line is the predicted correlation for a value of τ equal to 0.29 and Z equal to 35 when ionic strength is varied.

interaction model that includes only excluded volume and adhesive interactions, where the values of τ range from 0.17 to 10. The dashed line corresponds to the full potential of mean force model for a value of $\tau = 0.29$ and protein net charge Z equal to 35. As mentioned previously, when only short-ranged interactions are included in the model, the correlation line has a slope equal to 1.03. This is similar to the experimental slope equal to 1.06 when a range of antibodies at low and high ionic strength are included in the data set.[34] When electrostatic interactions are included in the model there is a slight positive curvature to the correlation. This curvature would be difficult to detect experimentally and most likely would be reflected by linear correlations with slopes slightly greater than 1.03. Very good agreement with the calculated correlation is obtained for solutions where protein−protein repulsion is screened, especially considering that there are no fit parameters and the simplifying spherical assumptions used in the model.

Recent studies on antibody solutions have rationalized the behavior of k_D in terms of[77]

$$k_D = 2BM - \bar{v} - \psi \tag{43}$$

where $\bar{v}$ is the practical specific volume of the protein and ψ is the first order coefficient in protein concentration for the expansion of the sedimentation coefficient or the friction coefficient

$$f = f_0(1 + \psi c) \tag{44}$$

f is the friction coefficient at protein concentration c and f_0 is the infinite dilution value. For hard spheres, eq 43 is equivalent to eq 24, where[77]

$$-\psi = k_O + k_A + k_S + k_{FD} + \bar{v} \tag{45}$$

The concentration dependence of the frictional coefficient is related to only hydrodynamic interactions because sedimentation is driven by an external field. The main contribution of protein−protein interactions to the frictional coefficient is

dx.doi.org/10.1021/mp5002334 | Mol. Pharmaceutics XXXX, XXX, XXX−XXX

contained in the Oseen term; for short-ranged interactions $k_O^{sr} = -0.5k_V^{sr}$ and for electrical double layer forces, $k_O^{el} \approx -0.5k_V^{el}$. Thus, changing solution conditions will have a similar effect on the sedimentation and diffusion interaction parameters, because both will be proportional to the change in the Oseen interaction parameter k_O. The predicted behavior is consistent with a sedimentation velocity study of lysozyme where changes in ψ with increasing ionic strength correlated with a similar decrease in k_D.[1]

DISCUSSION

The main purpose of breaking up the protein−protein interaction into a simplified model are twofold. The first is to separate out the longer-ranged electrostatic interaction from the short-ranged adhesive force. The second purpose is to provide a link between the k_D and B_{22} measurements. In solutions at low pH, the validity of using the double layer potential has been demonstrated by obtaining accurate fits to the ionic strength dependence of protein−protein interactions. There are limitations to the approach because the charge determined from fitting the DLVO potential does not match what is expected from the ζ-potential measurements, but this is not surprising when a spherical shape and uniform charge distribution are used to describe an antibody. The approach only works well at low pH where repulsive electrostatics dominate. The deficiencies are clearly reflected by the presence of attractive electrostatic interactions in solutions at pH 9. The nonmonotonic ionic strength trend of protein−protein interactions at intermediate pH values between 7.25 and 8.5 can be rationalized by the competition between repulsive electrostatics at low ionic strength and attractive electrostatics above a critical ionic strength. For proteins carrying a net charge, attractive electrostatic interactions arise when the net protein−protein interation is dominated by a small number of low energy configurations corresponding to surfaces with charge complementarity. When the protein−protein interactions are repulsive, there is less weighting of attractive configurations in favor of sampling the large ensemble of repulsive orientations. Thus, the nonmonotonic behavior provides evidence for a transition from a centrosymmetric protein−protein interaction to an orientationally constrained (anisotropic) interaction at the critical ionic strength. What is not known is whether electrostatic or nonelectrostatic forces determine the low energy protein configurations sampled above the critical ionic strength. The measured pH and ionic strength patterns for k_D follow the same trends as those observed from a combined numerical and theoretical study of charged dipolar spheres indicating that the behavior is reconcilable in terms of electrostatic effects.[71] However, the experimentally observed maxima in protein−protein attraction occur at a higher ionic strength, which might reflect an enhancement of the electrostatic attraction by other short-ranged forces. The results presented here indicate that small changes in either ionic strength or pH can lead to a switch from repulsive to attractive electrostatic interactions.

We have shown that the same correlation between B_{22} and k_D is obtained if the protein−protein interaction is only composed of a short-ranged electrostatic repulsion versus a short-ranged attractive interaction as described by the Baxter adhesive potential. Indeed the correlation is more broadly applicable and is independent of the mathematical form of the pair potential as long as the force remains short-ranged since slight deviations in the correlation occur when long-ranged electrostatics were included in the potential model. Thus, approximating the protein as a sphere within the Baxter model likely works because the correlation between k_D and B_{22} is independent of the details of the pair potential. That is, when the pair potential between nonspherical sticky particles is angle-averaged, the potential of mean force with respect to separation will become more rugged but remain short-ranged as long as the particles are not elongated. However, one assumption that has not been tested here is whether the short-ranged attractive interaction is anisotropic. A similar approach could be taken using a model spherical particle with a fixed number of interacting sites, each characterized by the same stickiness parameter, to test whether an anisotropic model can also capture the generic behavior of the correlation between B_{22} and k_D.

ASSOCIATED CONTENT

Supporting Information

Comparison of the screened Yukawa potential to a numerical solution obtained using Deryaguin's method. This material is available free of charge via the Internet at http://pubs.acs.org.

AUTHOR INFORMATION

Corresponding Author

*E-mail: r.curtis@manchester.ac.uk.

Notes

The authors declare no competing financial interest.

ACKNOWLEDGMENTS

Dorota Roberts was supported by a BRIC/BBSRC Grant Number BB/I017194/1. Robin Curtis had an ISS grant from the Royal Academy of Engineering that supported his part-time placement in 2013 at MedImmune. The authors thank Wyatt Technology for continued instrument support and helpful discussions, in particular, Kevin Jackson, Dan Some, and Sophia Kenrick. mAb1 was kindly supplied by MedImmune.

REFERENCES

(1) Saluja, A.; Fesinmeyer, R. M.; Hogan, S.; Brems, D. N.; Gokarn, Y. R. Diffusion and Sedimentation Interaction Parameters for Measuring the Second Virial Coefficient and Their Utility as Predictors of Protein Aggregation. *Biophys. J.* **2010**, *99*, 2657−2665.

(2) Saito, S.; Hasegawa, J.; Kobayashi, N.; Kishi, N.; Uchiyama, S.; Fukui, K. Behavior of Monoclonal Antibodies: Relation Between the Second Virial Coefficient (B_2) at Low Concentrations and Aggregation Propensity and Viscosity at High Concentrations. *Pharm. Res.* **2012**, *29*, 397−410.

(3) He, F.; Woods, C. E.; Becker, G. W.; Narhi, L. O.; Razinkov, V. I. High-Throughput Assessment of Thermal and Colloidal Stability Parameters for Monoclonal Antibody Formulations. *J. Pharm. Sci.* **2011**, *100*, 5126−5141.

(4) Mason, B. D.; Zhang, L.; Remmele, J.; Richard, L.; Zhang, J. Opalescence of an IgG2 Monoclonal Antibody Solution as it Relates to Liquid-Liquid Phase Separation. *J. Pharm. Sci.* **2011**, *100*, 4587−4596.

(5) Mason, B. D.; Zhang-van Enk, J.; Zhang, L.; Remmele, R. L.; Zhang, J. Liquid-Liquid Phase Separation of a Monoclonal Antibody and Nonmonotonic Influence of Hofmeister Anions. *Biophys. J.* **2010**, *99*, 3792−3800.

(6) Salinas, B. A.; Sathish, H. A.; Bishop, S. M.; Harn, N.; Carpenter, J. F.; Randolph, T. W. Understanding and Modulating Opalescence and Viscosity in a Monoclonal Antibody Formulation. *J. Pharm. Sci.* **2010**, *99*, 82−93.

(7) Nishi, H.; Miyajima, M.; Nakagami, H.; Noda, M.; Uchiyama, S.; Fukui, K. Phase Separation of an IgG1 Antibody Solution under a Low Ionic Strength Condition. *Pharm. Res.* **2010**, *27*, 1348−1360.

(8) Ahamed, T.; Esteban, B. N. A.; Ottens, M.; van Dedem, G. W. K.; van der Wielen, L. A. M.; Bisschops, M. A. T.; Lee, A.; Pham, C.; Thommes, J. Phase behavior of an intact monoclonal antibody. *Biophys. J.* **2007**, *93*, 610−619.
(9) Lewus, R. A.; Darcy, P. A.; Lenhoff, A. M.; Sandler, S. I. Interactions and Phase Behavior of a Monoclonal Antibody. *Biotechnol. Prog.* **2011**, *27*, 280−289.
(10) Sukumar, M.; Doyle, B. L.; Combs, J. L.; Pekar, A. H. Opalescent appearance of an IgG1 antibody at high concentrations and its relationship to noncovalent association. *Pharm. Res.* **2004**, *21*, 1087−1093.
(11) Jezek, J.; Rides, M.; Derham, B.; Moore, J.; Cerasoli, E.; Simler, R.; Perez-Ramirez, B. Viscosity of concentrated therapeutic protein compositions. *Adv. Drug Delivery Rev.* **2011**, *63*, 1107−1117.
(12) Saluja, A.; Badkar, A. V.; Zeng, D. L.; Kalonia, D. S. Ultrasonic rheology of a monoclonal antibody (IgG(2)) solution: Implications for physical stability of proteins in high concentration formulations. *J. Pharm. Sci.* **2007**, *96*, 3181−3195.
(13) Yadav, S.; Shire, S. J.; Kalonia, D. S. Viscosity behavior of high-concentration monoclonal antibody solutions: Correlation with interaction parameter and electroviscous effects. *J. Pharm. Sci.* **2012**, *101*, 998−1011.
(14) Liu, J.; Nguyen, M. D. H.; Andya, J. D.; Shire, S. J. Reversible self-association increases the viscosity of a concentrated monoclonal antibody in aqueous solution. *J. Pharm. Sci.* **2005**, *94*, 1928−1940.
(15) Yadav, S.; Shire, S. J.; Kalonia, D. S. Factors Affecting the Viscosity in High Concentration Solutions of Different Monoclonal Antibodies. *J. Pharm. Sci.* **2010**, *99*, 4812−4829.
(16) Kanai, S.; Liu, J.; Patapoff, T. W.; Shire, S. J. Reversible self-association of a concentrated monoclonal antibody solution mediated by Fab-Fab interaction that impacts solution viscosity. *J. Pharm. Sci.* **2008**, *97*, 4219−4227.
(17) Connolly, B. D.; Petry, C.; Yadav, S.; Demeule, B.; Ciaccio, N.; Moore, J. M. R.; Shire, S. J.; Gokarn, Y. R. Weak Interactions Govern the Viscosity of Concentrated Antibody Solutions: High-Throughput Analysis Using the Diffusion Interaction Parameter. *Biophys. J.* **2012**, *103*, 69−78.
(18) Neergaard, M. S.; Kalonia, D. S.; Parshad, H.; Nielsen, A. D.; Moller, E. H.; van de Weert, M. Viscosity of high concentration protein formulations of monoclonal antibodies of the IgG1 and IgG4 subclass - Prediction of viscosity through protein-protein interaction measurements. *Eur. J. Pharm. Sci.* **2013**, *49*, 400−410.
(19) Chi, E. Y.; Krishnan, S.; Kendrick, B. S.; Chang, B. S.; Carpenter, J. F.; Randolph, T. W. Roles of conformational stability and colloidal stability in the aggregation of recombinant human granulocyte colony-stimulating factor. *Protein Sci.* **2003**, *12*, 903−913.
(20) Olsen, S. N.; Andersen, K. B.; Randolph, T. W.; Carpenter, J. F.; Westh, P. Role of electrostatic repulsion on colloidal stability of *Bacillus halmapalus* alpha-amylase. *Biochim. Biophys. Acta, Proteins Proteomics* **2009**, *1794*, 1058−1065.
(21) Saito, S.; Hasegawa, J.; Kobayashi, N.; Tomitsuka, T.; Uchiyama, S.; Fukui, K. Effects of Ionic Strength and Sugars on the Aggregation Propensity of Monoclonal Antibodies: Influence of Colloidal and Conformational Stabilities. *Pharm. Res.* **2013**, *30*, 1263−1280.
(22) Le Brun, V.; Friess, W.; Bassarab, S.; Muhlau, S.; Garidel, P. A critical evaluation of self-interaction chromatography as a predictive tool for the assessment of protein-protein interactions in protein formulation development: A case study of a therapeutic monoclonal antibody. *Eur. J. Pharm. Biopharm.* **2010**, *75*, 16−25.
(23) Jimenez, M.; Rivas, G.; Minton, A. P. Quantitative characterization of weak self-association in concentrated solutions of immunoglobulin G via the measurement of sedimentation equilibrium and osmotic pressure. *Biochemistry* **2007**, *46*, 8373−8378.
(24) Pathak, J. A.; Sologuren, R. R.; Narwal, R. Do Clustering Monoclonal Antibody Solutions Really Have a Concentration Dependence of Viscosity? *Biophys. J.* **2013**, *104*, 913−923.
(25) Chari, R.; Jerath, K.; Badkar, A. V.; Kalonia, D. S. Long- and Short-Range Electrostatic Interactions Affect the Rheology of Highly Concentrated Antibody Solutions. *Pharm. Res.* **2009**, *26*, 2607−2618.
(26) Yadav, S.; Liu, J.; Shire, S. J.; Kalonia, D. S. Specific Interactions in High Concentration Antibody Solutions Resulting in High Viscosity. *J. Pharm. Sci.* **2010**, *99*, 1152−1168.
(27) Kumar, V.; Dixit, N.; Zhou, L. L.; Fraunhofer, W. Impact of short range hydrophobic interactions and long range electrostatic forces on the aggregation kinetics of a monoclonal antibody and a dual-variable domain immunoglobulin at low and high concentrations. *Int. J. Pharm.* **2011**, *421*, 82−93.
(28) Neal, B. L.; Asthagiri, D.; Velev, O. D.; Lenhoff, A. M.; Kaler, E. W. Why is the osmotic second virial coefficient related to protein crystallization? *J. Cryst. Growth* **1999**, *196*, 377−387.
(29) Elcock, A. H.; McCammon, J. A. Calculation of weak protein-protein interactions: The pH dependence of the second virial coefficient. *Biophys. J.* **2001**, *80*, 613−625.
(30) Song, X. Y.; Zhao, X. F. The van der Waals interaction between protein molecules in an electrolyte solution. *J. Chem. Phys.* **2004**, *120*, 2005−2009.
(31) Pellicane, G.; Smith, G.; Sarkisov, L. Molecular Dynamics Characterization of Protein Crystal Contacts in Aqueous Solutions. *Phys. Rev. Lett.* **2008**, *101*, No. 248102.
(32) McManus, J. J.; Lomakin, A.; Ogun, O.; Pande, A.; Basan, M.; Pande, J.; Benedek, G. B. Altered phase diagram due to a single point mutation in human gamma D-crystallin. *Proc. Natl. Acad. Sci. U.S.A* **2007**, *104*, 16856−16861.
(33) Yadav, S.; Laue, T. M.; Kalonia, D. S.; Singh, S. N.; Shire, S. J. The Influence of Charge Distribution on Self-Association and Viscosity Behavior of Monoclonal Antibody Solutions. *Mol. Pharmaceutics* **2012**, *9*, 791−802.
(34) Lehermayr, C.; Mahler, H.-C.; Maeder, K.; Fischer, S. Assessment of Net Charge and Protein-Protein Interactions of Different Monoclonal Antibodies. *J. Pharm. Sci.* **2011**, *100*, 2551−2562.
(35) Felderhof, B. U. Diffusion of Interacting Brownian Particles. *J. Phys. A: Math. Gen.* **1978**, *11*, 929−937.
(36) Kuehner, D. E.; Heyer, C.; Ramsch, C.; Fornefeld, U. M.; Blanch, H. W.; Prausnitz, J. M. Interactions of lysozyme in concentrated electrolyte solutions from dynamic light-scattering measurements. *Biophys. J.* **1997**, *73*, 3211−3224.
(37) Batchelor, G. K. Brownian Diffusion of Particles With Hydrodynamic Interaction. *J. Fluid Mech.* **1976**, *74*, 1−29.
(38) Phillies, G. D. J. Numerical Interpretation of the Concentration-dependence of Micelle Diffusion-coefficients. *J. Colloid Interface Sci.* **1987**, *119*, 518−523.
(39) Ooi, T. Light Scattering From Multi-component Systems. *J. Polym. Sci.* **1958**, *28*, 459−462.
(40) Casassa, E. F.; Eisenberg, H. Thermodynamic Analysis of Multicomponent Solutions. *Adv. Protein Chem.* **1964**, *19*, 287−395.
(41) Vrij, A.; Overbeek, J. T. Scattering of Light By Charged Colloidal Particles In Salt Solutions. *J. Colloid. Sci.* **1962**, *17*, 570−&.
(42) Berne, B.; Pecora, R. *Dynamic Light Scattering, With Applications to Chemistry, Biology, and Physics*; John Wiley & Sons: New York, 1976.
(43) Delgado, A. V.; Gonzalez-Caballero, E.; Hunter, R. J.; Koopal, L. K.; Lyklema, J. Measurement and interpretation of electrokinetic phenomena - (IUPAC technical report). *Pure Appl. Chem.* **2005**, *77*, 1753−1805.
(44) Warwicker, J. Continuum Dielectric Modeling of the Protein Solvent System, and Calculation of the Long-range Electrostatic-field of the Enzyme Phosphoglycerate Mutase. *J. Theor. Biol.* **1986**, *121*, 199−210.
(45) Neal, B. L.; Asthagiri, D.; Lenhoff, A. M. Molecular origins of osmotic second virial coefficients of proteins. *Biophys. J.* **1998**, *75*, 2469−2477.
(46) Gruenberger, A.; Lai, P.-K.; Blanco, M. A.; Roberts, C. J. Coarse-Grained Modeling of Protein Second Osmotic Virial Coefficients: Sterics and Short-Ranged Attractions. *J. Phys. Chem. B* **2013**, *117*, 763−770.
(47) Rosenbaum, D.; Zamora, P. C.; Zukoski, C. F. Phase behavior of small attractive colloidal particles. *Phys. Rev. Lett.* **1996**, *76*, 150−153.

(48) Piazza, R.; Peyre, V.; Degiorgio, V. "Sticky hard spheres" model of proteins near crystallization: A test based on the osmotic compressibility of lysozyme solutions. *Phys. Rev. E* **1998**, *58*, R2733−R2736.
(49) Tardieu, A.; Le Verge, A.; Malfois, M.; Bonnete, F.; Finet, S.; Ries-Kautt, M.; Belloni, L. Proteins in solution: From X-ray scattering intensities to interaction potentials. *J. Cryst. Growth* **1999**, *196*, 193−203.
(50) Zhang, F.; Roth, R.; Wolf, M.; Roosen-Runge, F.; Skoda, M. W. A.; Jacobs, R. M. J.; Stzucki, M.; Schreiber, F. Charge-controlled metastable liquid-liquid phase separation in protein solutions as a universal pathway towards crystallization. *Soft Matter* **2012**, *8*, 1313−1316.
(51) Hunter, R. J. *Foundations of Colloid Science*; Oxford University Press: New York, 2001.
(52) Arzensek, D.; Kuzman, D.; Podgornik, R. Colloidal interactions between monoclonal antibodies in aqueous solutions. *J. Colloid Interface Sci.* **2012**, *384*, 207−216.
(53) Muschol, M.; Rosenberger, F. Interactions in undersaturated and supersaturated lysozyme solutions: Static and dynamic light scattering results. *J. Chem. Phys.* **1995**, *103*, 10424−10432.
(54) Curtis, R. A.; Prausnitz, J. M.; Blanch, H. W. Protein-protein and protein-salt interactions in aqueous protein solutions containing concentrated electrolytes. *Biotechnol. Bioeng.* **1998**, *57*, 11−21.
(55) Eberstein, W.; Georgalis, Y.; Saenger, W. Molecular-interactions In Crystallizing Lysozyme Solutions Studied By Photon-correlation Spectroscopy. *J. Cryst. Growth* **1994**, *143*, 71−78.
(56) Petsev, D. N.; Denkov, N. D. Diffusion of Charged Colloidal Particles At Low-volume Fraction - Theoretical-model and Light-scattering Experiments. *J. Colloid Interface Sci.* **1992**, *149*, 329−344.
(57) Zhang, L.; Tan, H.; Fesinmeyer, R. M.; Li, C.; Catrone, D.; Le, D.; Remmele, J.; Richard, L.; Zhang, J. Antibody solubility behavior in monovalent salt solutions reveals specific anion effects at low ionic strength. *J. Pharm. Sci.* **2012**, *101*, 965−977.
(58) Medda, L.; Barse, B.; Cugia, F.; Bostrom, M.; Parsons, D. F.; Ninham, B. W.; Monduzzi, M.; Salis, A. Hofmeister Challenges: Ion Binding and Charge of the BSA Protein as Explicit Examples. *Langmuir* **2012**, *28*, 16355−16363.
(59) Goto, Y.; Takahashi, N.; Fink, A. L. Mechanism of Acid-induced Folding of Proteins. *Biochemistry* **1990**, *29*, 3480−3488.
(60) Ramos, C. H. I.; Baldwin, R. L. Sulfate anion stabilization of native ribonuclease A both by anion binding and by the Hofmeister effect. *Protein Sci.* **2002**, *11*, 1771−1778.
(61) Ebel, C.; Faou, P.; Kernel, B.; Zaccai, G. Relative role of anions and cations in the stabilization of halophilic malate dehydrogenase. *Biochemistry* **1999**, *38*, 9039−9047.
(62) Sedlak, E.; Stagg, L.; Wittung-Stafshede, P. Effect of Hofmeister ions on protein thermal stability: Roles of ion hydration and peptide groups? *Arch. Biochem. Biophys.* **2008**, *479*, 69−73.
(63) Dubin, S. B.; Clark, N. A.; Benedek, G. B. Measurement of Rotational Diffusion Coefficient of Lysozyme By Depolarized Light Scattering: Configuration of Lysozyme In Solution. *J. Chem. Phys.* **1971**, *54*, 5158−5164.
(64) Abramo, M. C.; Caccamo, C.; Costa, D.; Pellicane, G.; Ruberto, R.; Wanderlingh, U. Effective interactions in lysozyme aqueous solutions: A small-angle neutron scattering and computer simulation study. *J. Chem. Phys.* **2012**, *136*, 035103.
(65) Blanco, M. A.; Sahin, E.; Li, Y.; Roberts, C. J. Reexamining protein-protein and protein-solvent interactions from Kirkwood-Buff analysis of light scattering in multi-component solutions. *J. Chem. Phys.* **2011**, *134*, No. 225103.
(66) Dumetz, A. C.; Chockla, A. M.; Kaler, E. W.; Lenhoff, A. M. Effects of pH on protein-protein interactions and implications for protein phase behavior. *Biochim. Biophys. Acta, Proteins Proteomics* **2008**, *1784*, 600−610.
(67) Dumetz, A. C.; Snellinger-O'Brien, A. M.; Kaler, E. W.; Lenhoff, A. M. Patterns of protein - protein interactions in salt solutions and implications for protein crystallization. *Protein Sci.* **2007**, *16*, 1867−1877.
(68) Tessier, P. M.; Johnson, H. R.; Pazhianur, R.; Berger, B. W.; Prentice, J. L.; Bahnson, B. J.; Sandler, S. I.; Lenhoff, A. M. Predictive crystallization of ribonuclease A via rapid screening of osmotic second virial coefficients. *Proteins* **2003**, *50*, 303−311.
(69) Velev, O. D.; Kaler, E. W.; Lenhoff, A. M. Protein interactions in solution characterized by light and neutron scattering: Comparison of lysozyme and chymotrypsinogen. *Biophys. J.* **1998**, *75*, 2682−2697.
(70) Piazza, R.; Iacopini, S.; Galliano, M. BLGA protein solutions at high ionic strength: Vanishing attractive interactions and "frustrated" aggregation. *Europhys. Lett.* **2002**, *59*, 149−154.
(71) Bratko, D.; Striolo, A.; Wu, J. Z.; Blanch, H. W.; Prausnitz, J. M. Orientation-averaged pair potentials between dipolar proteins or colloids. *J. Phys. Chem. B* **2002**, *106*, 2714−2720.
(72) Phillies, G. D. Excess Chemical Potential of Dilute-solutions of Spherical Polyelectrolytes. *J. Chem. Phys.* **1974**, *60*, 2721−2731.
(73) Persson, B. A.; Jonsson, B.; Lund, M. Enhanced Protein Steering: Cooperative Electrostatic and van der Waals Forces in Antigen-Antibody Complexes. *J. Phys. Chem. B* **2009**, *113*, 10459−10464.
(74) Grigsby, J. J.; Blanch, H. W.; Prausnitz, J. M. Cloud-point temperatures for lysozyme in electrolyte solutions: effect of salt type, salt concentration and pH. *Biophys. Chem.* **2001**, *91*, 231−243.
(75) Broide, M. L.; Tominc, T. M.; Saxowsky, M. D. Using phase transitions to investigate the effect of salts on protein interactions. *Phys. Rev. E* **1996**, *53*, 6325−6335.
(76) Seyrek, E.; Dubin, P. L.; Tribet, C.; Gamble, E. A. Ionic strength dependence of protein-polyelectrolyte interactions. *Biomacromolecules* **2003**, *4*, 273−282.
(77) Harding, S. E.; Johnson, P. The Concentration-dependence of Macromolecular Parameters. *Biochem. J.* **1985**, *231*, 543−547.